# 6

# Anisotropic Diffusion: From the Apparent Diffusion Coefficient to the Apparent Diffusion Tensor

PETER J. BASSER AND EVREN ÖZARSLAN

**Summary Box**

- Characterizing water diffusion within soft tissues at the micron-length scale is aided by using the concepts of the apparent diffusion coefficient (ADC) and apparent diffusion tensor (ADT).
- The ADT generalizes the ADC, allowing one to characterize both heterogeneous and anisotropic diffusion, observed in many ordered media and tissues.
- The NMR measurement of the ADT (i.e., DT-NMR) generalizes the earlier NMR measurement of the ADC (i.e., diffusion NMR).
- The MRI measurement of the ADT (i.e., DTI) generalizes the earlier MRI measurement of the ADC (i.e., diffusion MRI).
- Many useful intrinsic parameters can be derived from the ADT that help characterize local microstructure.
- The size, shape, and orientation of the diffusion ellipsoid, obtained from the ADT, are useful to visualize features of local tissue microstructure.
- Diffusion tensor fields, measured via diffusion tensor imaging (DTI), can be used to generate models of fiber tracts and fiber pathways (e.g., DTI tractography).
- More complex representations of water diffusion in tissue can extend the sensitivity and selectivity of diffusion MRI beyond that provided by DTI.

As we have seen in previous chapters (Chapter 4 by Callaghan, and Chapter 5 by Le Bihan), nuclear magnetic resonance (NMR) is the gold standard for measuring the diffusivity of water and other spin-labeled species. It is the least perturbing measurement imaginable, providing extremely accurate and precise data. We have also learned that the subsequent combination of the Stejskal and Tanner pulsed-field gradient (PFG) NMR sequence with an MRI sequence allows diffusion measurements to be performed on a voxel-by-voxel basis.

MRI measurement of water diffusivity in soft tissue provides unique useful biological and clinical information about tissue composition, the physical properties of tissue constituents, tissue microstructure, and its architectural organization. Moreover, this information can be obtained in vivo, noninvasively without the



06-Jones-Chap-06.indd 79 8/2/2010 5:25:59 PM

need to introduce contrast agents, since the water protons (or other molecule) whose random motion is being characterized are ones within the tissue itself.

However, in order to characterize diffusive transport in tissue and other complex media, several additional concepts beyond the self-diffusivity (the diffusion coefficient of the solute in the same solvent) need to be introduced. In tissue, the *solute* water is no longer diffusing within the *solvent* water alone. While tissue is composed mainly of water, it also contains biopolymers (primarily proteins, glycoproteins, and lipids) with numerous distinct cellular and subcellular microcompartments and separate domains having different physical and chemical environments. Thus, we need to extend the concept of self-diffusivity to treat diffusive transport meaningfully in such a complex medium.

In this chapter, we will review the concept of the apparent diffusion coefficient (ADC), as a generalization of self-diffusivity, and then further generalize the ADC to be able to describe anisotropic or orientationally dependent water diffusion in fibrous media such as nerve white matter. This brings us to the concept of the apparent diffusion tensor (ADT).

## Isotropic Self-Diffusion

We have seen earlier that isotropic diffusion, which occurs in pure liquids, describes the finding that the self-diffusivity is the same in all directions. So, a single self-diffusion coefficient is sufficient to describe the transport properties caused by random thermal collisions among molecules.

## Apparent Diffusion Coefficient

In more complex media, however, such as gels, colloids, polymeric solutions, and some biological tissue (e.g., skeletal muscle), Tanner (1966, 1978, 1979, 1983) recognized that self-diffusivity was no longer sufficient to describe diffusive transport. When a solute molecule is not only colliding with like molecules but also reflecting from impermeable barriers or moving into regions having different polymer or matrix volume fractions, the self-diffusion concept does not apply. To address this deficiency, Tanner introduced the notion of the apparent diffusion coefficient (ADC) to the NMR community. Simply put, the ADC is the diffusivity one would calculate using the Stejskal and Tanner formula if the displacement distribution were Gaussian. Le Bihan later brought the ADC concept to the diffusion MRI community and proposed that perfusion in the microvasculature could result in intravoxel incoherent motion (IVIM) (Le Bihan et al., 1986), contributing an additional source of spin dephasing, and signal attenuation not considered by Tanner.

## Diffusion Anisotropy

*Anisotropy* means that a property of a material takes on different values when it is measured along different directions. *Diffusion anisotropy* simply means that the measured diffusivity is not the same in all directions, i.e., it is not directionally uniform (isotropic) as it would be for water diffusing in a jar of water.

In some tissues and fibrous media, the observation of macroscopic diffusion anisotropy is a result of an underlying ordered microstructural organization that persists on the scale of the sample volume (e.g., the imaging voxel). In such media, we expect diffusion transport properties to vary with orientation since water molecules are likely to encounter different barriers and obstacles according to the direction in which they move. (In Chapter 7, Beaulieu provides a comprehensive look at the possible causes of diffusion anisotropy in the peripheral and central nervous system [CNS]). Characterizing diffusion anisotropy quantitatively can provide information about not only the direction along which these fibers are aligned but also often the organization and properties of its ordered elements.

In a biological context, anisotropic diffusion was first observed in NMR experiments performed on skeletal muscle (Cleveland et al., 1976; Tanner, 1979). Interest in this phenomenon, however, was rekindled when it was observed in MRIs of animal and human brains (Chenevert et al., 1990; Douek et al., 1991; Moseley et al., 1990a, 1991; Moonen et al., 1991; Sakuma et al., 1991). Characterization or measurement of diffusion anisotropy with NMR requires a more elaborate mathematical framework and experimental design than conventional diffusion NMR.

## Diffusion NMR vs. Diffusion Tensor NMR

A reasonable starting point is to compare and contrast diffusion NMR with diffusion tensor NMR. Diffusion NMR is based on a *one-dimensional* model of molecular displacements. Specifically, the measurement of an ADC is obtained from the *projection* of all molecular displacements onto the axis along which the diffusion gradients are applied. In this case, the term *apparent diffusion coefficient* is apt, since, microscopically, although diffusion occurs only along one direction, the ADC is non-zero for all directions except the one perpendicular to the direction of motion (see Basser and Pajevic, 2004, for more explanation). So, there appears to be diffusion in all directions but it is only taking place along one.

Tanner (1977) proposed the following formula to relate the ADC to the measured NMR signal:

$$\ln\left(\frac{A(b)}{A(b=0)}\right) = -b\,\mathrm{ADC} \qquad [6.1]$$

Above, $A(b)$ is the echo magnitude of the diffusion-weighted signal and $A(b = 0)$ is the echo magnitude of the non–diffusion-weighted signal, and $b$ is the $b$-factor (see Eq. [5.6] of the previous chapter by Le Bihan). In tissues, such as brain gray matter, where the ADC (measured on the scale of the typical imaging voxel used in clinical diffusion-weighted imaging) is largely independent of the orientation of the tissue, a single ADC is often sufficient to characterize the diffusion process at the voxel scale. However, in anisotropic media, such as skeletal and cardiac muscle (Cleveland et al., 1976; Tanner, 1979; Garrido et al., 1994) and in white matter (Moseley et al., 1990a, 1991; Turner et al., 1990; Henkelman et al., 1994), where the ADC depends on the orientation of the tissue, the one-dimensional (1D) Gaussian model is inadequate to characterize the orientation-dependent water mobility.

A more general description of anisotropic free diffusion uses a *three-dimensional* (3D) Gaussian model of molecular displacements, which contains a symmetric effective or apparent diffusion *tensor* (ADT) of water, **D** (e.g., see Crank, 1975), in place of a scalar ADC to describe the orientation dependence of diffusion. In essence, diffusion tensor NMR consists of the measurement of **D** (and functions of it) from a series of diffusion-weighted NMR signals. **D** is determined by using a relationship between the measured echo signal in each voxel and the applied magnetic field gradient sequence (Basser et al., 1994a; Mattiello et al., 1994,

1995, 1997), which was derived from Stejskal's classic solution to the modified Bloch-Torrey equation given in Appendix 6A (Stejskal and Tanner, 1965):

$$\ln\left(\frac{A(\mathbf{b})}{A(\mathbf{b}=\mathbf{0})}\right)=-\left(b_{xx}D_{xx}+2b_{xy}D_{xy}+2b_{xz}D_{xz}+b_{yy}D_{yy}+2b_{yz}D_{yz}+b_{zz}D_{zz}\right) \quad [6.2]$$

Above, $A(\mathbf{b})$ is the echo magnitude of the diffusion-weighted signal, $A(\mathbf{b} = \mathbf{0})$ is the echo magnitude of the non–diffusion-weighted signal, and $b_{ij}$ is a component of the symmetric b-matrix, **b**. In diffusion NMR, a scalar *b*-factor is calculated for each DW signal. In diffusion tensor NMR, a symmetric b-matrix is calculated for each DW signal. Just as in diffusion NMR one uses a collection of DW signals and their corresponding *b*-factors to estimate an ADC using linear regression, in diffusion tensor NMR, one uses a collection of DW signals and their corresponding b-matrices to estimate **D** using weighted multivariate linear regression of Eq. [6.1]. In Figure 6.1, we illustrate the components of the diffusion tensor computed for a human brain data set. Chapter 16 by Koay covers many numerical aspects of this estimation problem, and Chapter 20 by Pajevic describes some of the statistical properties of the estimated **D** as well as some tensor-derived parameters.

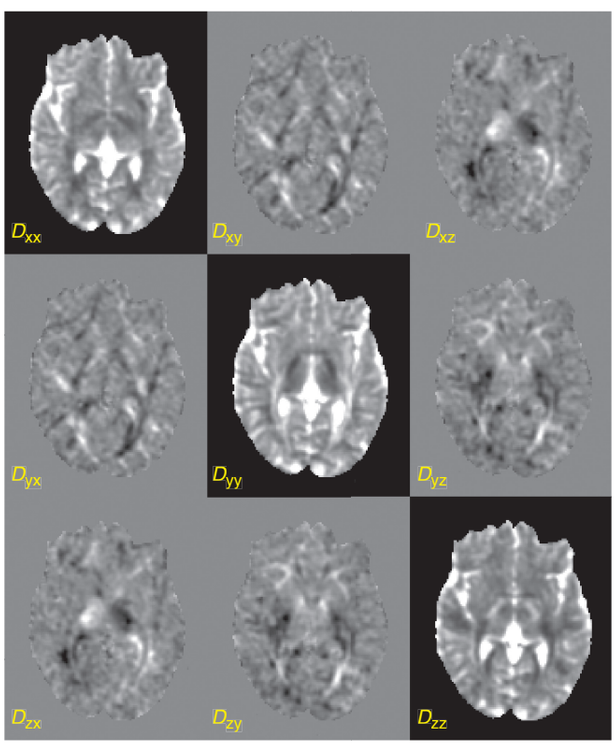


**Figure 6.1** A diffusion tensor image of the human brain. Here, each image depicts another component of the diffusion tensor. The diagonal components ($D_{xx}$, $D_{yy}$, and $D_{zz}$) are scaled between 0 and $1.5 \times 10^{-3}$ mm²/s whereas the off-diagonal components ($D_{xy}$, $D_{xz}$, $D_{yz}$, $D_{yx}$, $D_{zx}$, and $D_{zy}$) are scaled between $-4 \times 10^{-3}$ mm²/s and $4 \times 10^{-3}$ mm²/s. Note that as a consequence of the symmetry of the tensor, $D_{xy}$=$D_{yx}$, $D_{xz}$=$D_{zx}$, and $D_{yz}$=$D_{zy}$.

It is easy to see that the diffusion tensor NMR model reduces to the diffusion NMR model in the limiting case when the medium is isotropic. In this case, the 3D Gaussian model assumed in diffusion tensor NMR reduces to the 1D Gaussian model assumed in diffusion NMR. Then, $D_{xx} = D_{yy} = D_{zz}$ = ADC, and $D_{xy} = D_{xz} = D_{yz} = 0$, and Eq. [6.2] reduces to Eq. [6.1]

$$\ln\left(\frac{A(\mathbf{b})}{A(\mathbf{b}=\mathbf{0})}\right)=-b\ \mathrm{ADC} \quad [6.3]$$

with the *b*-factor given by the Trace of the symmetric b-matrix, i.e., $b = b_{xx} + b_{yy} + b_{zz}$ = Trace(**b**).

However, there are important differences between the designs of diffusion and diffusion tensor NMR experiments. For diffusion experiments, it is sufficient to apply diffusion gradients along only one direction, whereas for diffusion tensor experiments, one must apply diffusion gradients along at least six non-collinear, non-coplanar directions (Basser et al., 1994a) to be able to estimate all six diagonal and off-diagonal elements of **D**.

## Geometric Representation of the Translational Apparent Diffusion Tensor in 3D

An intuitive way to understand the meaning of **D** is to perform various Gedanken experiments in which we follow the Brownian motion of an ensemble of "tagged" water molecules released from the center of a voxel, as shown for one molecule in the cartoon in Figure 6.2. If we imagine performing this experiment in a jar of water, the rate of diffusive transport will be the same in all directions. Diffusion is then said to be *isotropic* and is completely specified by a single scalar self-diffusion constant, *D*. Thus, diffusion isotropy describes the case in which the molecular diffusivity is independent of the medium's orientation. For a diffusion time, Δ, the translational displacement distribution is spherically symmetric, and surfaces of constant probability or water concentration are

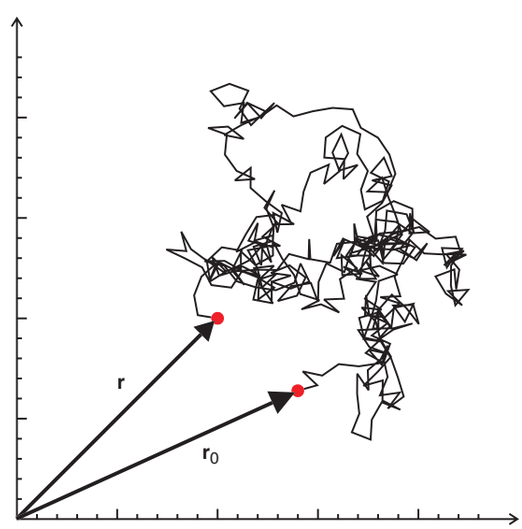


**Figure 6.2** The Brownian picture of diffusion is best epitomized by the cartoon above illustrating a possible path taken by a molecule that is released at point $\mathbf{r}_0$ at time $t = 0$ and moves to position **r** at a later time, *t*. The molecule undergoes a "drunken walk" whose random motion is described by a displacement probability distribution.

concentric spheres. When considering the Einstein (1926) formula for 1D diffusion

$$\left\langle x^2 \right\rangle = 2D\Delta \qquad [6.4]$$

we can construct a sphere whose radius equals the root mean-squared (rms) displacement of water molecules after diffusion time Δ, a graphical representation of which can be found in Figure 6.3a.

If we now perform the same Gedanken experiment in a liquid crystalline medium or a system with microscopically aligned rods, the rate of diffusive transport will no longer be the same in all directions. Diffusion anisotropy implies that the translational displacement probability of the diffusing species is now biased, depending on the medium's orientation. In homogeneous (i.e., spatially uniform) anisotropic media, the voxel-averaged displacement distribution is given by:

$$P\left(\mathbf{R},\Delta \middle| 0,0\right) = \frac{1}{\sqrt{|\mathbf{D}|\,(4\pi\Delta)^3}} e^{\frac{-\mathbf{R}^T\,\mathbf{D}^{-1}\,\mathbf{R}}{4\Delta}} \qquad [6.5]$$

where the column vector $\mathbf{R} = (x,y,z)^T$ is the net displacement, and $|\mathbf{D}|$ is the determinant of **D**. The covariance matrix, $2\Delta\mathbf{D}$, characterizes the shape of the displacement distribution. In Appendix 6B we establish the correspondence between the covariance matrix for the displacements and the diffusion tensor using a random walk scheme. Surfaces of constant probability or particle concentration can be obtained by setting the exponent in Eq. [6.5] to a constant. Note that in order for the above expression to tend to zero for large displacements, all quadratic forms of the diffusion tensor have to be positive, i.e., **D** has to be a positive definite tensor. Then this equation describes a three-dimensional ellipsoid in displacement space, called the "diffusion ellipsoid" (Stejskal, 1965; Crank 1975; Basser et al., 1994a), whose *size*, *shape*, and *orientation* embody important features of anisotropic Gaussian diffusion.

One can always rotate the laboratory ($x$-$y$-$z$) coordinate axes so that they are aligned with the local principal ($x'$-$y'$-$z'$) axes of the diffusion ellipsoid in each voxel. As described in Appendix 6B, the diagonal elements of the diffusion tensor are proportional to the second moment of displacements along the three coordinate axes, whereas the off-diagonal elements yield the correlation between displacements along orthogonal directions. In the preferred principal frame of reference, displacements along the three new axes are decoupled, and all off-diagonal elements of **D** vanish. Then the exponent of the displacement distribution takes on a simpler form:

$$\left(\frac{x'}{\sqrt{2\lambda_{x'}\Delta}}\right)^2 + \left(\frac{y'}{\sqrt{2\lambda_{y'}\Delta}}\right)^2 + \left(\frac{z'}{\sqrt{2\lambda_{z'}\Delta}}\right)^2 \qquad [6.6]$$

Above, $\lambda_{x'}$ $\lambda_{y'}$ and $\lambda_{z'}$ are the three principal diffusivities (or eigenvalues), corresponding to the three respective principal directions, $\varepsilon_{x'}$, $\varepsilon_{y'}$, and $\varepsilon_{z'}$; $\sqrt{2\lambda_{x'}\Delta}$, $\sqrt{2\lambda_{y'}\Delta}$, and $\sqrt{2\lambda_{z'}\Delta}$ are the root mean-squared (rms) displacements along these three principal directions at diffusion time, Δ, respectively. Figure 6.3b illustrates typical prolate and oblate diffusion ellipsoids. The lengths of the major and minor axes of the diffusion ellipsoid represent these three distances. In turbid biological tissue, the direction of the principal ($x'$-$y'$-$z'$) axes of the diffusion ellipsoid are generally not known a priori, and typically do not coincide with the laboratory coordinate system. In general, it is necessary to assume that they are different in each voxel (Basser et al., 1994a).

In summary, both diagonal and off-diagonal elements of **D** measured in diffusion tensor NMR are essential to characterize the probability distribution in Eq. [6.5] as well as in characterizing the size, shape, and orientation of the diffusion ellipsoid constructed from **D**.

## Quantitative Parameters Provided by Diffusion Tensor NMR

Scalar parameters that embody distinct intrinsic features listed above, such as descriptors of the size and shape of the diffusion ellipsoid, should be *rotationally invariant*, i.e., independent of the orientation of the anisotropic structure, the orientation of the specimen with respect to the laboratory coordinate system, the applied diffusion sensitizing gradients, and even the choice of the laboratory coordinate system in which the components of **D** and the magnetic field gradients are measured (Basser and Le Bihan, 1992; Basser et al., 1994b). Rotational invariance is a necessary condition for a tensor-derived quantity to be intrinsic to the medium.

Possibly the most important rotationally invariant quantitative scalar parameters provided by diffusion tensor NMR are the three eigenvalues, $\lambda_1$, $\lambda_2$, and $\lambda_3$ (i.e., the eigenvalues of **D** described above, $\lambda_{x'}$ $\lambda_{y'}$ and $\lambda_{z'}$, but sorted according to size). We use

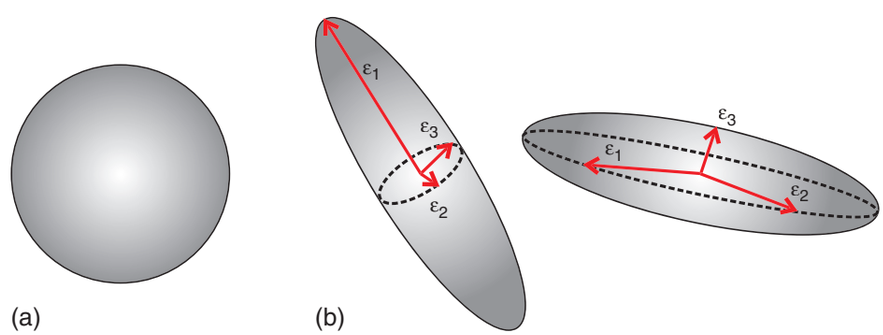


**Figure 6.3** **a)** In isotropic media, the root mean squared (rms) displacement or diffusion ellipsoid is spherical. **b)** However, in anisotropic media, the diffusion ellipsoid is either prolate or oblate, and its three principal directions are coincident with the eigenvectors of **D**, $\varepsilon_1$, $\varepsilon_2$, and $\varepsilon_3$.

different functions of the eigenvalues to characterize the size and shape of the diffusion ellipsoid. The orientational information describing the anisotropic diffusion process is encoded by the three corresponding eigenvectors of **D**.

## Size of the Diffusion Ellipsoid

Quantities described below characterize the size of the diffusion ellipsoid, independent of orientation and shape. The first scalar valued map of interest is an image with no diffusion weighting, i.e., the $A(b = 0)$ map discussed above. This image is shown on the left panel of Figure 6.4. By far the most important diffusion tensor NMR-derived quantity turns out to be the simplest:

$$\mathrm{Trace}(\mathbf{D}) = D_{xx} + D_{yy} + D_{zz} = 3\langle D\rangle = \lambda_1 + \lambda_2 + \lambda_3 = 3\langle\lambda\rangle \quad [6.7]$$

Physically, Trace(**D**) is three times the orientationally averaged diffusivity, $\langle D\rangle$, which can be also be obtained by arithmetically averaging the ADC distribution uniformly over all possible directions (Kärger et al., 1988; Özarslan et al., 2005). Trace(**D**) is intrinsic to the tissue; it is independent of fiber orientation, gradient directions, etc.

This independence of fiber orientation has made Trace(**D**) a clinically valuable parameter, particularly in monitoring stroke and other neurological disorders, as described in other chapters. Moseley and colleagues discovered in animals (Moseley et al., 1990b, 1990c, 1990d) and Warach et al. (1992, 1995) later showed in humans that a reduction of the ADC in brain parenchyma can be used to track the onset and assess the severity of a cerebral ischemic event (see Chapter 31 by Wu, Nentwich, Chutinet, and Bayrlee). Moreover, an elevation in ADC was observed in chronic stroke, often associated with the development of lacunar infarcts (see Chapter 32 by O'Sullivan). Thus, it seemed possible to follow an acute stroke in progress, and the subsequent chronic degeneration it caused using the ADC. However in white matter, because the signal attenuation and the ADC were seen to depend on the direction of the diffusion sensitizing gradient with respect to local nerve fiber orientation (Chenevert et al., 1990; Doran et al., 1990; Moseley et al., 1990a), it was generally not possible to determine the cause of an observed drop or recovery in the DW signal or ADC. Was it a result of a physiological or structural change in the tissue (brought on by the ischemic event itself) or a consequence of the relative orientation of white matter tracts and the applied diffusion gradient? In ischemia-monitoring applications, diffusion anisotropy in white matter was considered a confounding factor producing directionally dependent DWI signal intensities, thus complicating their clinical interpretation (for a personal perspective and historical account on this, the reader is referred to Chapter 46 by Moseley).

The use of Trace(**D**) effectively solved the "problem" of diffusion anisotropy in white matter that the use of the ADC along a single direction created. Because Trace (**D**) measures an intrinsic property of the medium, it is inherently insensitive to both the direction of the diffusion-sensitizing gradients and the orientation of white matter in a voxel (Basser and Le Bihan, 1992). Thus, displaying Trace(**D**) or $\langle D\rangle$ instead of an ADC measured along a particular direction eliminates all orientational dependence. In this way, observed changes in Trace(**D**) can be ascribed solely to changes in the tissue's structure or physiological state and no longer to its underlying diffusion anisotropy.

It is safe to say that the use of $\langle D\rangle$ in acute and chronic stroke assessment is still probably the most important and pervasive clinical application of DTI, although it is not widely appreciated that Trace(**D**) and $\langle D\rangle$ (sometimes referred to as the "mean ADC") are actually diffusion tensor–derived parameters. Another reason for the success of the Trace or "mean ADC" in stroke assessment is the surprising and still unexplained finding that Trace(**D**) is fairly uniform in normal brain parenchyma (van Gelderen et al. 1994; Pierpaoli and Basser, 1996; Pierpaoli et al., 1996; Ulug et al., 1997) at $b$-values up to around 1000 s/mm$^2$. Remarkably, as shown in the second panel of Figure 6.4, Trace(**D**) has virtually the same value in both white and gray matter, even though these two tissues are markedly different in structure and composition. van Gelderen et al. (1994) were the first to demonstrate this finding in cats, and Ulug et al. (1997) later observed it in humans.

Another measure of the size of the diffusion ellipsoid is the determinant of the diffusion tensor. This quantity is proportional to the volume of the diffusion ellipsoid, but because it depends on the product of the eigenvalues, it is more susceptible to the deleterious effects of NMR noise. It is still useful to mention it for completeness.

## Shape of the Diffusion Ellipsoid

A scalar measure of diffusion anisotropy should characterize the shape of the three-dimensional diffusion ellipsoid, independent

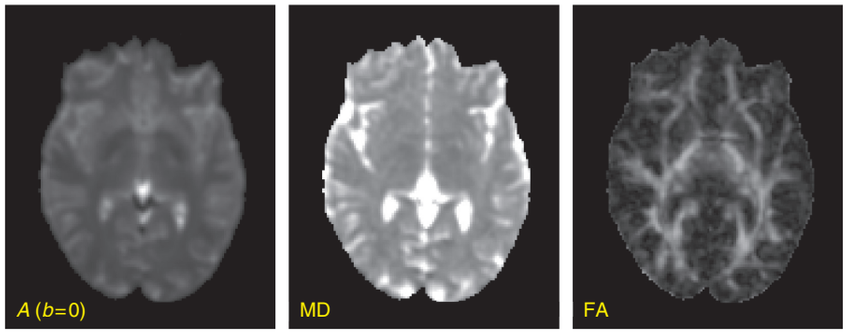


**Figure 6.4** Some orientationally invariant maps obtained from DTI of the human brain. On the left is a $T_2$-weighted map with no diffusion weighting obtained from the diffusion tensor fit to data. The center image shows a map of mean diffusivity (MD) whereas the last image on the right depicts the fractional anisotropy (FA) values.

of its orientation and size. Like the trace, such a measure should also be rotationally invariant, i.e., independent of the sample's placement or its orientation with respect to the (laboratory) *x-y-z* reference frame (Basser et al., 1994b). A good starting point is to consider the anisotropic part of **D**, or the "diffusion deviation tensor," in each voxel, ***D*** (Basser, 1995; Basser and Pierpaoli, 1996):

$$\boldsymbol{D} = \mathbf{D} - \langle D \rangle \mathbf{I} \qquad [6.8]$$

where above, we see the familiar mean diffusivity, $\langle D \rangle$, is multiplied by the identity tensor, **I**. In defining the deviation tensor, we simply subtract the isotropic part from **D**. What is left is the *anisotropic* part of **D**.

The magnitude of the diffusion deviation tensor, Trace($\boldsymbol{D}^2$), can be shown to be proportional to the sample variance of the eigenvalues or principal diffusivities (Basser, 1995):

$$1/3\ \mathrm{Trace}\left(\boldsymbol{D}^2\right) = \frac{\left(\lambda_1 - \langle\lambda\rangle\right)^2 + \left(\lambda_2 - \langle\lambda\rangle\right)^2 + \left(\lambda_3 - \langle\lambda\rangle\right)^2}{3} = \mathrm{Var}(\lambda) \qquad [6.9]$$

This quantity, which is also rotationally invariant, is used in several popular diffusion anisotropy measures, such as the relative anisotropy (RA) (Basser, 1995),

$$\mathrm{RA} = \frac{\sqrt{Var(\lambda)}}{\langle D \rangle} \qquad [6.10]$$

and the fractional anisotropy (*FA*) (Basser, 1995),

$$\mathrm{FA} = \frac{3}{\sqrt{2}} \frac{\sqrt{Var(\lambda)}}{\sqrt{\lambda_1^2 + \lambda_2^2 + \lambda_3^2}} \qquad [6.11]$$

Both the RA and the FA characterize the degree of "out-of-roundness" of the diffusion ellipsoid. The RA is the coefficient of variation of the eigenvalues. The FA, as its name suggests, measures the fraction of the diffusion tensor's total magnitude that is anisotropic (Basser, 1995). An FA-valued image of the human brain is shown in the right panel of Figure 6.4.

Another useful "shape" parameter is the third moment or skewness of the eigenvalues:

$$1/3\ \mathrm{Trace}\left(\boldsymbol{D}^3\right) = \frac{\left(\lambda_1 - \langle\lambda\rangle\right)^3 + \left(\lambda_2 - \langle\lambda\rangle\right)^3 + \left(\lambda_3 - \langle\lambda\rangle\right)^3}{3} = \mathrm{Skewness}(\lambda) \qquad [6.12]$$

When the skewness is *positive* the diffusion ellipsoid is prolate (i.e., cigar shaped—a shape observed in white matter fibers in the corpus callosum and in the pyramidal tract in monkeys [Pierpaoli and Basser, 1996] and in humans [Pierpaoli et al., 1996]). When it is *negative*, the diffusion ellipsoid is oblate (i.e., pancake-shaped—a shape observed in white matter in the subcortical white matter regions in the centrum semiovale in humans [Pierpaoli et al., 1996]). Higher moments of the distribution of eigenvalues of **D** can be calculated in order to characterize diffusion anisotropy more completely; however, typically noise in the NMR signal introduces enough bias in the estimates of the eigenvalues to make these higher-order statistics inaccurate. Background noise even causes the variance of the eigenvalues to be underestimated and it causes other measures of diffusion anisotropy to be overestimated, owing to a phenomenon called "eigenvalue repulsion" (Pierpaoli and Basser, 1996). This noise-induced bias is discussed in depth in Chapter 20 by Pajevic.

A discussion about anisotropy measures would not be complete without treating Westin et al.'s three novel tensor-derived parameters (Westin et al., 1999). The first one measures the degree to which **D** is line-like; the second, plane-like; and the third, sphere-like (corresponding to a decomposition of the diffusion tensor into diffusion ellipsoids that are prolate, oblate, and spherical, respectively). This tensor decomposition provides a useful geometric interpretation of the diffusion process. Despite the fact that these diffusion measures are not rotationally invariant (as are the three "moments" of **D**, the mean, variance, and skewness, described above), the planar measure, in particular, appears to have many desirable properties for identifying regions where the diffusion ellipsoid is oblate. The reader is referred to Chapter 21 by Leemans on visualization for more details and example maps.

## Orientation of Diffusion Ellipsoids and Their Spatial Distribution

Diffusion tensor NMR also provides orientational information given by the principal axes or the three orthogonal eigenvectors of the diffusion tensor. These quantities are extremely useful in characterizing the architecture of fibrous media, particularly fibrous tissues. It was proposed that in ordered fibrous tissues, the eigenvector associated with the largest eigenvalue within a voxel lies parallel to the local fiber direction (Basser et al., 1994b). As we will see below, this idea became the basis of several strategies for following nerve fibers in the brain, which were dubbed "tractography." Before we consider this application, however, we need to describe how to go from diffusion tensor NMR to diffusion tensor MRI.

### Diffusion Tensor NMR to Diffusion Tensor MRI

The migration of diffusion tensor NMR to diffusion tensor MRI follows very closely the migration of diffusion NMR to diffusion MRI. Both diffusion MRI and diffusion tensor MRI use the same diffusion-weighted MRIs (DWIs) as inputs, but as we have seen in the previous sections, the former uses the 1D Stejskal and Tanner equation to compute an ADC in each voxel, whereas the latter uses the diffusion tensor model to estimate an ADT in each voxel.

Other chapters in this book explain different facets of diffusion MRI, its underpinnings and its applications so there is no need to repeat this information here. We will assume the reader is familiar with the notion of a diffusion-weighted image (DWI) as well as conventional MRI pulse sequences used to acquire one (see Chapter 5 by Le Bihan). Familiarity with the formula used to calculate an ADC in each voxel from a set of DWIs is also assumed (again, see Chapter 5). The "*b*-factor" or "*b*-value" has also been introduced in this context as a measure of the degree of diffusion weighting in conventional diffusion MRI. Whereas the *b*-value summarizes the attenuating effect of diffusion and imaging gradients on the MR signal along one direction (Neeman et al., 1990), the b-matrix summarizes the attenuating effect of all gradient waveforms (i.e., all imaging and diffusion gradient sequences) applied in all three directions, x, y, and z (Basser et al., 1994a; Mattiello et al., 1997, 1995, 1994).

To implement diffusion tensor MRI effectively, one must further expand the notion of "cross-terms" (see the section Gradient Interactions, the *b*-Factor, and the b-Matrix in Chapter 5). Interactions between imaging and diffusion gradients applied in

orthogonal directions, and even between imaging gradients alone applied in orthogonal directions, can introduce additional diffusion weighting (Mattiello et al., 1994, 1997), i.e., signal loss. In isotropic media, however, interactions between gradients applied in orthogonal directions do not produce any diffusion attenuation, but in anisotropic media these interactions can result in additional diffusion attenuation.

The history of the development of diffusion tensor MRI did not follow the histories of other MRI modalities, such as the imaging or mapping of the ADC, $T_1$, $T_2$, magnetization transfer (MT), proton density, phase, and chemical shift. For each of these methods, there was already a spectroscopic method that had been invented and developed almost a half-century before their MRI counterpart. For DTI, however, there was no classical NMR method to measure the self-diffusion tensor or the effective (or apparent) diffusion tensor of water (or other species) in the laboratory coordinate frame. So, unlike $T_1$ MRI or DWI, implementing DTI first required developing diffusion tensor NMR (Basser et al., 1992; 1994a) and then combining it with conventional MRI (Basser et al., 1994b) to achieve diffusion tensor MRI.

## Exploring Diffusion Tensor Fields and Their Properties

Now that we are able to measure a diffusion tensor, and thus a diffusion ellipsoid, in each voxel within an imaging volume, we can consider making maps or images of all of the quantitative scalar and vector parameters described in the previous sections. In general, with this new spatial information, we are now able to characterize *fields* of diffusion ellipsoids and other tensor-derived quantities within an imaging volume. Some features involve the spatial rate of change of tensor-derived quantities within the imaging volume, such as the gradient of $\langle D \rangle$, or the gradient of the magnitude of the deviation tensor described above (Pajevic et al., 2002). The former provides information about the location of boundaries between cerebrospinal fluid (CSF) and tissue parenchyma, while the latter often (but not always) provides information about boundaries between white and gray matter. Typically, it is challenging to calculate these quantities from noisy, discrete, voxel-averaged DTI data, so some spatial smoothing, for example, using a continuous approximation to the diffusion tensor field (Pajevic et al., 2002) or a regularization scheme (Poupon et al., 1998), must be performed beforehand.

Imaging methods that apply this idea include direction field mapping, in which the local fiber direction (or more correctly, orientation) is displayed as a vector (or line segment) in each voxel, and fiber-tract color mapping, in which a color, assigned to a voxel containing anisotropic tissue, is used to signify the local fiber tract direction (Pajevic and Pierpaoli, 1999). An important achievement of color mapping has been the ability to identify unambiguously all major commissural, association and projection pathways in the human brain (Makris et al., 1997; Pajevic and Pierpaoli, 2000).

## DTI Fiber Tractography

DTI fiber tractography is a natural extension of diffusion ellipsoid imaging. In brain regions where the diffusion ellipsoids are prolate, indicative of well-ordered white matter fascicles, in which the purported fiber direction is slowly changing from voxel to voxel, we can imagine connecting the ends of these discrete ellipsoids into an extended object, like a link-sausage or natural-pearl necklace, depicting the trajectory of a large fiber tract. Blurring these diffusion ellipsoids, like what one does standing at the opposite end of a picture gallery when looking at a pointillist painting, leads naturally to the idea of diffusion tensor tractography. Your eye naturally joins diffusion ellipsoids into a continuous fiber tract.

*DTI fiber tractography* (Wedeen et al., 1995; Basser, 1998; Conturo et al., 1999; Jones et al., 1999; Mori et al., 1999; Poupon et al., 1999; Basser et al., 2000) is the name that we gave to the mathematical procedure to follow coherently ordered fiber tract trajectories within the brain and other fibrous tissues. Like color mapping, it is also based on the idea that in ordered fibrous tissues, the eigenvector associated with the largest eigenvalue within a voxel is parallel to the local fiber direction (Basser et al., 1994a). A review of this field is provided in Section 4 of this book (see Chapter 22 by Alexander and Chapter 23 by Parker).

Since its introduction, several different schemes have been proposed to follow fiber tracts. The earliest methods proposed for fiber-tract following were deterministic. In these so-called streamline approaches, fiber-tract trajectories are generated from the local fiber-tract direction field in much the same way fluid streamlines are generated from a fluid velocity field. Starting from a "seed point," fibers are launched in both directions until some stopping or "termination" criteria are satisfied, such as the FA dropping below its level in background noise. A *fiber tract* is the name given to all points along such a continuous trajectory. One disadvantage of this computational strategy is that errors can accumulate during the tract-following process. In general, one cannot be assured that the trajectories represent actual or even probable pathways of nerve fibers.

The second strategy is probabilistic (Parker, 2000; Tuch et al., 2000; Batchelor et al., 2001; Koch et al., 2001, 2002; Behrens et al., 2002; Parker et al., 2002). A seed point is assumed to be connected to all points within the imaging volume, but the most probable connections are those that minimize some cost function, such as the strain energy of the pathway (Tuch et al., 2000). This approach holds great promise in that many paths are explored, but only those that are frequently traversed are assigned a high likelihood. Of course, a disadvantage of this approach is that we do not know what physical constraints nature uses to construct nerve pathways. The development of probabilistic approaches that do not rely on functional minimization appear to be quite promising (Behrens et al., 2003), although further validation studies still should be performed.

A hybrid tractography method, proposed by Jones and Pierpaoli (2004), uses the streamline method in conjunction with an empirical statistical scheme, bootstrapping (see Pajevic and Basser, 2003), to generate many plausible fiber tract realizations. In this way, many possible paths can be generated from the same DWI data set and the variability of these paths can be assessed. This is done without making any assumptions about the source of artifacts in the DWIs. A disadvantage of this approach is that it generally requires acquiring more DWIs than is necessary for a typical DTI study, although recent advances in applying newer bootstrap approaches (e.g., the wild bootstrap [Jones, 2008]) may obviate acquiring additional data. Here the reader is referred to the Chapter 20 for more details on these statistical approaches.

It is important to note that a number of well-documented artifacts in DTI fiber tractography arise as discrete, coarsely sampled, noisy, voxel-averaged direction field data (Basser, 1998) and are used to reconstruct topologically complex nerve pathways (Pierpaoli et al., 2001). These artifacts can produce "phantom" connections between different brain regions that do not exist anatomically (a "false positive"), or they can result in missing anatomical

connections that do exist (a "false negative"). There are usually a number of thresholds and free parameters that can be set in existing tractography codes whose adjustment can alter one's findings. Therefore, great care must be exercised in obtaining "anatomical connectivity" with DTI fiber tractography (Basser et al., 2000). Clearly, skepticism is warranted when interpreting such data—less in the coherent primary pathways, but increasingly in finer and more complex white matter structures.

Artistically pleasing computer graphics–inspired schemes have been proposed to visualize fiber tract trajectories (Catani et al., 2002). Zhang et al. (2000, 2004) have used streamtubes to visualize fiber tract trajectories and streamsurfaces to visualize regions in which fibers cross within a plane. These imaginative strategies will find increased use in displaying features of high-dimensional data inherent in DTI. For an in-depth review of visualization strategies and glyphs used in diffusion MRI, the reader is referred to Chapter 21.

## Issues in Inferring Tissue Microstructure from the NMR Signal

Inferring the microstructure and the underlying architectural organization of tissue using diffusion imaging data has been a long sought-after goal; however, its attainment is complicated by several factors. First, the homogeneity of tissue within each voxel cannot be assumed. Numerous microscopic compartments exist in brain parenchyma. Typically, gray matter, white matter, and CSF can occupy the same voxel. The number of these distinct tissue types and their distribution within the voxel are generally not known a priori. At a microstructural level, gray and white matter are heterogeneous, having a distribution of macromolecular structures with a range of sizes, shapes, composition, and physical properties (such as $T_2$, $D$). Differences in relaxation parameters can lead to different rates of echo attenuation in each compartment, making it more difficult to explain the cause of signal loss within a voxel. There are also irregular boundaries between macromolecular and microscopic-scale compartments. Water diffusion may be restricted in some compartments and hindered in others (see Chapters 7, 8, and 9 for the difference between hindered and restricted diffusion). Some water will be associated with certain macromolecules while some will be free to diffuse. Another unknown is whether there is water exchange between compartments, which can also affect the relaxation rates of the spin system. Water movement within and between compartments is still not well understood, although tractable models exist to describe it. Owing to differences in blood flow and thermal conductivity, temperature cannot even be assumed to be uniform throughout a tissue sample. It is well known that temperature affects the measured diffusivity (Simpson and Carr, 1958; Mills, 1973; Le Bihan et al., 1989), typically by about 1.5% for each degree (°C) (Simpson and Carr, 1958).

The factors listed above partially explain why the underlying cause of diffusion anisotropy has not been fully elucidated in brain parenchyma, although at low $b$-values typical of DTI, most investigators ascribe it to ordered, heterogeneous structures, such as large oriented extracellular and intracellular macromolecules, supermacromolecular structures, organelles, and membranes. In the central nervous system (CNS), diffusion anisotropy is not caused simply by myelin in white matter, since it has been shown in several studies that even before myelin is deposited, diffusion anisotropy can be measured using MRI (Beaulieu and Allen, 1994a, 1994b; Wimberger et al., 1995; Neil et al., 1998; Beaulieu, 2002). Thus, despite the fact that increases in myelin are temporally correlated with increases in diffusion anisotropy, structures other than the myelin sheath must also be contributing to diffusion anisotropy. This is an important consideration, because there is a common misconception that the degree of diffusion anisotropy can be used as a quantitative measure or "stain" of myelin content, when no such simple relationship exists. The reader is referred to Chapter 7 by Beaulieu for a thorough treatise on the studies that have been performed to elucidate the causes of anisotropy in white matter.

Recently, with the advent of stronger magnetic field gradients, several groups, for example, Mulkern et al. (1999), have reported nonmonoexponential decay of the MR signal intensity as a function of $b$-value, and have attempted to infer from it properties of distinct tissue compartments. Putting aside the complexities of obtaining stable estimates of discrete exponentials (i.e., diffusion relaxography), numerous microstructural and architectural configurations could produce the same multiexponential relaxation data. For example, Peled showed that a system of impermeable tubes with a distribution of diameters consistent with those found in histological brain slices could give rise to multiexponential decay of the signal (Peled et al., 1999). Similar behavior is expected when there is a statistical distribution of any relevant physical property or microstructural dimension within a voxel. It is unlikely that a particular exponential in a multiexponential model of diffusion attenuation can ever meaningfully be assigned to a particular and distinct tissue compartment. Clearly, without invoking additional *a priori* information about tissue structure, tissue composition, the physical properties of the different compartments, and their spatial distribution, determining tissue microstructural and architectural features from the NMR signal remains a challenging, ill-posed, inverse problem. (For more on the biophysics of nonmonoexponential decay, the reader is referred to Chapter 8 by Ackerman and Neil.)

## Limitations of DTI

While DTI completely characterizes the Gaussian contribution of the water diffusion process within tissues (Basser, 2002b), there are a number of clear limitations and caveats when using the DTI framework in living tissues. First, in tissue regions where the fiber architecture is complex (i.e., not characterized by a uniform coherent fiber orientation in each voxel), the DTI model will provide only a voxel-averaged diffusion tensor, belying the more complex underlying fiber structure. Second, as $q$- (see Chapter 4) or $b$-values are increased, there is evidence that some of the measured diffusion signal arises from water that is trapped within compartments, such as in intra-axonal spaces (Assaf and Cohen, 2000). The Gaussian displacement model that is assumed in DTI does not adequately describe the displacement distribution of spins trapped within pores or closed domains ("restricted diffusion"). Operationally, as we will see in the next section, the "safe" regime to use the DTI model is when the signal attenuation is well described by the Gaussian displacement distribution, i.e., there is a linear dependence of the signal attenuation with $b$ or a quadratic dependence with $q$.

## Beyond DTI

Many new methods have been developed to characterize features of the non-Gaussian displacement profile observed at high $b$- or $q$-values. These new approaches include diffusion spectrum

imaging (DSI) (Wedeen et al., 2000), a variant of Callaghan's 3D k- and q-space MRI (Callaghan et al., 1988; Callaghan, 1991), high angular resolution diffusion imaging (HARDI) (Frank, 2001, 2002), persistent angular structure MRI (PAS-MRI) (Jansons and Alexander, 2003), generalized diffusion tensor MRI (GDTI) (Liu et al., 2003; Özarslan and Mareci, 2003), q-ball MRI (Tuch et al., 2003), composite hindered and restricted model of diffusion (CHARMED) MRI (Assaf et al., 2004), diffusion orientation transform (DOT) (Özarslan et al., 2006), and multitensor MRI (Clark and Le Bihan, 2000; Inglis et al., 2001). A detailed treatise on these methods and their applications can be found in Chapter 27, by Alexander and Seunarine, and Chapter 28, by Tournier.

First, as a general requirement, all of these methods must either subsume DTI or reduce to it in the limit of low $b$ (or low $q$), where the Gaussian diffusion model applies (Basser, 2002). Specifically, it is useful to examine the form of the DW-NMR signal in the limit as the "$q$" value approaches zero. In one dimension, one can write (see Eq. [4.36] in Chapter 4) (Callaghan et al., 1999)

$$\left|E\left(q_z,\Delta\right)\right| = \mathrm{Re}\left(\left\langle \mathrm{e}^{-\mathrm{i}2\pi q_z Z}\right\rangle\right) \approx 1 - 2\pi^2 q_z^2 \left\langle Z^2\right\rangle + O\left(q_z^4\right) \quad [6.13]$$

The NMR signal attenuation caused by random displacements projected along the $Z$ direction clearly shows a quadratic dependence on $q_z$ in the small-$q$ limit (Callaghan and Stepisnik, 1996; Callaghan et al., 1999). If one uses the Einstein equation, $\left\langle Z^2\right\rangle = 2D\Delta$, to define an effective diffusivity, $D$, then one immediately obtains

$$\left|E\left(q_z,\Delta\right)\right| \sim 1 - 4\pi^2 q_z^2 D\Delta + O\left(q_z^4\right) \quad [6.14]$$

It is straightforward to generalize this result to three dimensions (Basser, 2002):

$$\left|E\left(\mathbf{q},\Delta\right)\right| = 1 - 4\pi^2 \mathbf{q}^T \mathbf{D}\mathbf{q}\,\Delta + O\left(q^4\right) \quad [6.15]$$

To second order in $\mathbf{q}$, one cannot distinguish the decay of $|E(\mathbf{q})|$ in Eq. [6.15] to that produced by a 3D Gaussian displacement distribution for $\mathbf{r}$. This finding is also consistent with Stepisnik's (1999) analysis using the method of cumulants in the Gaussian limit. (For a thorough review of cumulant analysis, the reader is referred to Chapter 10 by Kiselev). Thus, in the regime in which $q$ is sufficiently small, we can always treat the quadratic decay of $|E(\mathbf{q})|$ vs. $q$ as arising from a Gaussian displacement distribution.

A second issue with using higher-order or more complex models of diffusion is that specifying them typically entails acquiring a greater number of DWIs having more gradient directions and/or a larger range of gradient strengths than are needed in DTI. In principle, while one may obtain more information, it is generally at the price of additional MR acquisition time. Although, as discussed in Chapter 15 by Jones, there are advantages to using more than the bare minimum of six directions, when encoding for DTI analysis (Jones, 2004) in applications such as the assessment of acute stroke, this additional price is unjustifiably high, particularly when it may be sufficient to produce a mean ADC map or even a DWI to provide the necessary clinical information. In a careful neurological assessment of fiber tract organization in the brain or a neuroscience-inspired study about anatomical connectivity, a detailed DTI study may not be sufficient and a higher-order model may be required. Clearly, the clinical or biological application or question suggests the appropriate displacement imaging method one should use.

Another important point is that the methods discussed above (including DTI) are all predicated on the assumption that each voxel in each DWI volume contains the same tissue mass. While this assumption is not necessarily satisfied in DTI, methods have been developed to correct tissue misregistration artifacts (e.g., see Rohde et al., 2004). However, the likelihood of tissues being misregistered increases as the number of DWIs increases and/or as the $b$-values increase. Other forms of distortion (particularly eddy current distortion) can become severe at high $b$-values, although some strategies have been proposed to ameliorate these (Reese et al., 2003). (A much more in-depth treatment of these issues is provided in Section 3 of this book). At high $b$-values, however, bulk and small-scale motion are difficult to correct, since there are so few landmarks to identify in heavily diffusion-weighted MRIs. Typically, since most of the signal attenuation is used to estimate $\mathbf{D}$, little is left over to characterize the non-Gaussian contribution. In this high-$b$ regime, noise becomes increasingly prominent in DWIs. The noise either has to be reduced or fitted so as not to introduce artifacts in the processed data. Recent work in the effects of noise in high–$b$-value DWI is given in Jones and Basser (2004). Collectively, these issues present serious technical challenges to all high $b$- or high $q$-methods, which will have to be ameliorated.

## Conclusion

The use of the ADC concept has allowed quantitative diffusion NMR experiments to be applied to fixed and living tissue, and the development of diffusion MRI has enabled the mapping of diffusion properties within such tissue. The proposal of the apparent diffusion tensor, or ADT, and an experimental design to estimate or measure it extends the applicability of diffusion NMR and MRI data to complex anisotropic tissues, while still using the same diffusion-weighted NMR and MRI signals as before. This development has led to the estimation of a diffusion tensor in each voxel and mapping of a large number of useful, quantitative parameters derived from it.

DTI provides a means to probe tissue structure at different levels of hierarchical organization. While experimental diffusion times (i.e., milliseconds) are associated with mean-squared displacements of water molecules on the order of microns, these molecular motions are then averaged within a millimeter-scale voxel and then subsequently assembled into an image volume on a meter-length scale that encompasses entire organs and even the whole body. This integration over many length scales permits us to study and elucidate complex structural features of tissue from the macromolecular to the macroscopic. Various DTI-derived parameters described above, such as maps of the eigenvalues of the diffusion tensor, its trace, measures of the degree of diffusion anisotropy and organization, estimates of fiber direction, and white matter tract trajectory provide a unique multiscale description of tissue architecture and organization.

### Acknowledgments

The Intramural Research Program of the Eunice Kennedy Shriver National Institute of Child Health and Human Development supported this work. Several people deserve special recognition for their contributions to this chapter. Thanks go to Raisa Freidlin for reading and reviewing our manuscripts, and to Liz Salak for editing this manuscript.

## Appendix 6A

In this appendix, we provide a detailed derivation of the relationship between the diffusion-weighted MR signal and the diffusion tensor, following the development of Stejskal (1965). We start from the Bloch equations (Bloch, 1946) with Torrey's inclusion of relaxation due to diffusion (Torrey, 1956). This Bloch-Torrey equation relates the applied magnetic field vector, $\mathbf{B} = (B_x, B_y, B_z)$ to the net (nuclear) magnetization vector, $\mathbf{M} = (M_x, M_y, M_z)$ in the laboratory frame of reference:

$$\frac{\partial \mathbf{M}}{\partial t} = \gamma \mathbf{M} \times \mathbf{B} - \begin{pmatrix} T_2^{-1} & 0 & 0 \\ 0 & T_2^{-1} & 0 \\ 0 & 0 & T_1^{-1} \end{pmatrix} \mathbf{M} + \mathbf{M}_0 \begin{pmatrix} 0 \\ 0 \\ T_1^{-1} \end{pmatrix} + \nabla \cdot (\mathbf{D} \nabla \mathbf{M}). \quad [6A.1]$$

Above, $\gamma$ is the gyromagnetic ratio, $T_1$ and $T_2$ are the longitudinal and transverse relaxation times, and $\mathbf{M}_0$ is the equilibrium magnetization in the direction of the static applied magnetic field, $\mathbf{B}_0$. Here, we consider that the spins are subjected to an impressed static magnetic field, $B_0$, applied along the $z$-direction.

We also consider a Hahn spin-echo sequence (Hahn, 1950) in which linear, time-varying pulsed-field gradients (PFG) $\mathbf{G}(t)$, can be applied (Stejskal and Tanner, 1965). Then, the total magnetic field, $\mathbf{B}(\mathbf{r}, t)$, as a function of position and time is given by

$$\mathbf{B}(\mathbf{r}, t) = \left(0, 0, \mathbf{r} \cdot \mathbf{G}(t) + \mathbf{B}_0\right)^{\mathrm{T}} \quad [6A.2]$$

where $\mathbf{r}$ is the displacement vector, and

$$\mathbf{G}(t) = \left(G_x(t), G_y(t), G_z(t)\right)^{\mathrm{T}}. \quad [6A.3]$$

If we substitute complex transverse magnetization, $m(\mathbf{r},t)$,

$$m(\mathbf{r}, t) = M_x(\mathbf{r}, t) + iM_y(\mathbf{r}, t) \quad [6A.4]$$

then the Bloch-Torrey equation can be recast as a magnetization transport equation for $m$:

$$\frac{\partial m}{\partial t} = -i\omega_0 m - \frac{m}{T_2} - i\gamma \mathbf{r} \cdot \mathbf{G}(t) m + \nabla \cdot (\mathbf{D} \nabla m) \quad [6A.5]$$

where the Larmor equation, $\gamma B_0 = \omega_0$, was used.

To eliminate the attenuation due to transverse relaxation and signal modulation by Larmor precession, Stejskal and Tanner used the following substitution:

$$m(\mathbf{r}, t) = \psi(\mathbf{r}, t) \exp\left(-\left(i\omega_0 + \frac{1}{T_2}\right)t\right) \quad [6A.6]$$

so that

$$\frac{\partial \psi}{\partial t} = -i\gamma \mathbf{r} \cdot \mathbf{G}(t) \psi + \nabla \cdot (\mathbf{D} \nabla \psi) \quad [6A.7]$$

For a spin-echo sequence, one can further simplify the transport equation by separating $\psi(\mathbf{r}, t)$ into an imaginary part, which represents the solution to Eq. [6A.7] without diffusion, and a real, time-dependent part that represents the attenuation due to diffusion:

$$\psi(\mathbf{r}, t) = M(t) \exp(-i\mathbf{r} \cdot \mathbf{k}(t)) \quad [6A.8]$$

where

$$\mathbf{k}(t) = \gamma \int_0^t \mathbf{G}(t') dt'. \quad [6A.9]$$

The resulting ordinary differential equation for $M(t)$ is

$$\frac{\partial M}{\partial t} = M(t) \nabla \cdot \left(\mathbf{D} \exp(-i\mathbf{r} \cdot \mathbf{k}(t))\right) = -M(t)\, \mathbf{k}(t)^T \mathbf{D} \mathbf{k}(t) \quad [6A.10]$$

which has a solution for a homogeneous, anisotropic, infinite medium:

$$M(t) = M(0) \exp\left(-\int_0^t \mathbf{k}(u)^T \mathbf{D} \mathbf{k}(u) du\right) \quad [6A.11]$$

Above, $M(0)$ is the amplitude of the initial transverse magnetization (at $t = 0^+$) just after the 90° pulse is applied.

For an isotropic medium, the echo intensity, $M(TE)$, in a spin-echo experiment is then given by

$$\frac{M(TE)}{M(0)} = \exp\left(-D \int_0^{TE} \mathbf{k}(t') \cdot \mathbf{k}(t') dt'\right). \quad [6A.12]$$

This relation is valid for a PFG spin-echo sequence. After the 180° RF refocusing pulse, the sign of $\mathbf{G}$ is inverted (see Callaghan's discussion of the "effective gradient" [Callaghan, 1991]).

Le Bihan promoted the use of the "$b$-factor" to characterize the degree of diffusion weighting in DWI sequences (Le Bihan, 1991):

$$b = \int_0^{TE} \mathbf{k}(t') \cdot \mathbf{k}(t') dt'. \quad [6A.13]$$

For the 1D or isotropic diffusion case, the signal attenuation reduces to a simpler expression:

$$\frac{M(TE)}{M(0)} = \exp(-bD). \quad [6A.14]$$

One must remember that Eq. [6A.16] is strictly valid for diffusion in infinite, homogeneous, and isotropic media. Then, no cross-terms exist between gradient pulses—i.e., the contributions to the measured NMR signal from each gradient axis are uncoupled and may be determined separately (Mattiello et al., 1995). If diffusion is anisotropic, additional cross-terms must be taken into account in both diffusion spectroscopy (Basser et al., 1994a) and imaging (Mattiello et al., 1994, 1995, 1997).

In anisotropic diffusion, the apparent diffusion coefficient is replaced by an apparent or effective diffusion tensor (Basser et al., 1994a). In this situation, Eq. [6A.14] is no longer valid and the diffusion equations must be rewritten using a tensor formulation. The term $\mathbf{k}(t) \cdot \mathbf{k}(t)\, D$ in Eq. [6A.12] is replaced by the quadratic form, $\mathbf{k}(t)^{\mathrm{T}}\, \mathbf{D}\, \mathbf{k}(t)$. Eq. [6A.11] is used in place of Eq. [6A.12]. The echo attenuation then becomes

$$\frac{M(TE)}{M(0)} = \exp\left(-\sum_{i=1}^{3} \sum_{j=1}^{3} b_{ij} D_{ij}\right) \quad [6A.15]$$

where $b_{ij}$ is the $i$-$j^{\text{th}}$ component b-matrix, and $D_{ij}$ is the $i$-$j^{\text{th}}$ component of the effective or apparent diffusion tensor (Basser et al., 1994a). The diagonal elements, $D_{xx}$, $D_{yy}$, and $D_{zz}$, reflect correlations between molecular displacements in the same directions,

whereas the off-diagonal elements, $D_{xy}$, $D_{xz}$, $D_{yz}$, reflect correlations between molecular displacements in orthogonal directions that arise when not observing the diffusion process in the principal frame of reference. For instance, when observing diffusion in a pack or impermeable cylinders surrounded by an aqueous bathing medium with the cylinders' main axes oriented obliquely with respect to the *x*- and *y*-axes, net displacements measured along *x* will appear to be correlated to displacements along *y*, whereas, in the principal frame, they will not, and the off-diagonal elements vanish.

In general, when performing diffusion tensor NMR or MRI in turbid biological tissue, we must assume that both diagonal and off-diagonal elements in the diffusion tensor do not vanish, unless we know a priori that the gradient (laboratory coordinate) directions coincide with the principal directions of the material—a condition that is rarely satisfied, especially in NMR imaging applications.

## Appendix 6B

The main goal of this appendix is to derive the diffusion tensor from a random walk–based approach to diffusion and associate a meaning to the elements of the diffusion tensor. To this end, we provide a brief review of Markoff's method and apply it to the problem of random flights. The derivation follows closely the description as reviewed by Chandrasekhar (1943).

Let us assume that we have a single particle undergoing a series of random flights. At each step of its motion, the particle moves a distance $\mathbf{r}_k = (x_k, y_k, z_k)^T$ with a probability distribution function specified by $w_k(\mathbf{r}_k)$. After *N* such steps, the probability of finding the particle at the final position

$$\mathbf{R} = \sum_{k=1}^{N} \mathbf{r}_k \qquad [6B.1]$$

relative to the initial position is given by (Chandrasekhar, 1943):

$$Q_N(\mathbf{R}) = \frac{1}{8\pi^3} \int e^{-i\mathbf{K}\cdot\mathbf{R}} A_N(\mathbf{K})\, d\mathbf{K} \qquad [6B.2]$$

where

$$A_N(\mathbf{K}) = \prod_{k=1}^{N} \int w_k(\mathbf{r}_k) \mathbf{e}^{-i\mathbf{K}\cdot\mathbf{r}_k} \qquad [6B.3]$$

We shall assume that the probability density for each of the discrete jumps is identical, i.e., $w = w_k$ for all *k*. Employing the further assumption that all first moments of the displacements are zero, the $A_N(\mathbf{K})$ function takes the limiting form

$$A_N(\mathbf{K}) = \exp\left(-\frac{1}{2}\mathbf{K}^T\mathbf{S}\mathbf{K}\right) \qquad [6B.4]$$

as $N \to \infty$, where

$$S = \begin{pmatrix} \langle x^2 \rangle & \langle xy \rangle & \langle xz \rangle \\ \langle xy \rangle & \langle y^2 \rangle & \langle yz \rangle \\ \langle xz \rangle & \langle yz \rangle & \langle z^2 \rangle \end{pmatrix} \qquad [6B.5]$$

The components of this matrix are given by

$$S_{ij} = \langle r_i r_j \rangle = N \int r_i r_j w(\mathbf{r}) d\mathbf{r} \qquad [6B.6]$$

with $r_1 = x$, $r_2 = y$, and $r_3 = z$. The above form of the $A_N(\mathbf{K})$ function leads to the resulting probability distribution function

$$Q_N(\mathbf{R}) = \frac{1}{(8\pi^3 |\mathbf{S}|)^{1/2}} \exp\left(-\frac{1}{2}\mathbf{R}^T\mathbf{S}^{-1}\mathbf{R}\right) \qquad [6B.7]$$

Comparing this expression with Eq. [6.5] reveals the relationship between the diffusion tensor, **D**, and the matrix of variances, **S**, to be

$$\mathbf{D} = \frac{1}{2\Delta}\mathbf{S} \qquad [6B.8]$$

This is consistent with the proposed relationship between the diffusion tensor and the matrix of covariances provided in Basser (2002).

### References


Assaf Y, Cohen Y (2000). Assignment of the water slow-diffusing component in the central nervous system using q-space diffusion MRS: implications for fiber tract imaging. *Magn Reson Med* 43(2):191–9.

Assaf Y, Freidlin RZ, Rohde GK, Basser PJ (2004). New modeling and experimental framework to characterize hindered and restricted water diffusion in brain white matter. *Magn Reson Med* 52(5):965–978.

Basser PJ (1995). Inferring microstructural features and the physiological state of tissues from diffusion-weighted images. *NMR Biomed* 8(7-8): 333–344.

Basser PJ (1998). Fiber-tractography via diffusion tensor MRI (DT-MRI). Paper read at the 6th annual meeting of the ISMRM, April 18–24, 1998, Sydney, Australia.

Basser PJ (2002a). Diffusion tensor and q-space MR are complementary and consistent methodologies. Paper read at the 10th annual meeting of the ISMRM, Honolulu, Hawaii.

Basser PJ (2002b). Relationships between diffusion tensor and q-space MRI. *Magn Reson Med* 47(2):392–397.

Basser PJ, Le Bihan D (1992). Fiber orientation mapping in an anisotropic medium with NMR diffusion spectroscopy. Paper read at the 11th annual meeting of the SMRM, Berlin.

Basser PJ, Mattiello J, Le Bihan D (1992). Diagonal and off-diagonal components of the self-diffusion tensor: their relation to and estimation from the NMR spin-echo signal. Paper read at the 11th annual meeting of the SMRM, Berlin.

Basser PJ, Mattiello J, Le Bihan D (1994a). Estimation of the effective self-diffusion tensor from the NMR spin echo. *J Magn Reson Ser B* 103(3):247–254.

Basser PJ, Mattiello J, Le Bihan D. (1994b). MR diffusion tensor spectroscopy and imaging. *Biophys. J.* 66 (1):259–67.

Basser PJ, Mattiello J, Pierpaoli C, Le Bihan D (1994c). MR diffusion tensor imaging of ischemic brain in vivo. Paper read at 16th annual meeting of the IEEE EMBS, November 3, Baltimore, MD.

Basser PJ, Pajevic S, Pierpaoli C, Duda J, Aldroubi A (2000). In vivo fiber-tractography in human brain using diffusion tensor MRI (DT-MRI) data. *Magn Reson Med* 44(4):625–632.

Basser PJ, Pierpaoli C (1996). Microstructural and physiological features of tissues elucidated by quantitative-diffusion-tensor MRI. *J Magn Reson Ser B* 111(3):209–219.

Basser PJ, Pajevic S (2004). The problem with peanuts. Paper read at the 12th ISMRM Annual Meeting, Kyoto, Japan.

Batchelor PG, Hill DLG, Calamante F, Atkinson D (2001). Study of connectivity in the brain using the full diffusion tensor from MRI. Paper read at the 17th International Conference, IMPI.

Beaulieu C (2002). The basis of anisotropic water diffusion in the nervous system—a technical review. *NMR Biomed* 15(7-8):435–455.

Beaulieu C, Allen PS (1994a). Determinants of anisotropic water diffusion in nerves. *Magn Reson Med* 31(4):394–400.

Beaulieu C, Allen PS (1994b). Water diffusion in the giant axon of the squid: implications for diffusion-weighted MRI of the nervous system. *Magn Reson Med* 32(5):579–583.

Behrens TE, Woolrich MW, Jenkinson M, Johansen-Berg H, Nunes RG, Clare S, Matthews PM, Brady JM, Smith SM (2003). Characterization

and propagation of uncertainty in diffusion-weighted MR imaging. *Magn Reson Med* 50(5):1077–1088.

Behrens TEJ, Jenkinson M, Brady JM, Smith SM (2002). A probabilistic framework for estimating neural connectivity from diffusion weighted MRI. Paper read at ISMRM, Honolulu, Hawaii.

Bloch F (1946). Nuclear induction. *Phys Rev* 70(7 and 8):460–474.

Callaghan PT (1991). *Principles of Nuclear Magnetic Resonance Microscopy*. Oxford, UK: Oxford University Press.

Callaghan PT, Codd SL, Seymour JD (1999). Spatial coherence phenomena arising from translational spin motion in gradient spin echo experiments. *Concepts Magn Reson* 11(4):181–202.

Callaghan PT, Eccles CD, Xia Y (1988). NMR microscopy of dynamic displacements: k-space and q-space imaging. *J Phys E Sci Instrum* 21:820–822.

Callaghan PT, Stepisnik J (1996). Generalized analysis of motion using magnetic field gradients. *Adv Magn Reson* 19:325–388.

Catani M, Howard RJ, Pajevic S, Jones DK (2002). Virtual in vivo interactive dissection of white matter fasciculi in the human brain. *Neuroimage* 17(1):77–94.

Chandrasekhar S (1943). Stochastic problems in physics and astronomy. *Rev Mod Phys* 15(1):1–89.

Chenevert TL, Brunberg JA, Pipe JG (1990). Anisotropic diffusion in human white matter: demonstration with MR techniques in vivo. *Radiology* 177(2):401–405.

Clark CA, Le Bihan D (2000). Water diffusion compartmentation and anisotropy at high b values in the human brain. *Magn Reson Med* 44(6): 852–859.

Cleveland GG, Chang DC, Hazlewood CF, Rorschach HE (1976). Nuclear magnetic resonance measurement of skeletal muscle: anisotropy of the diffusion coefficient of the intracellular water. *Biophys J* 16(9): 1043–1053.

Conturo TE, Lori NF, Cull TS, Akbudak E, Snyder AZ, Shimony JS, McKinstry RC, Burton H, Raichle ME (1999). Tracking neuronal fiber pathways in the living human brain. *Proc Natl Acad Sci U S A* 96(18):10422–10427.

Crank J (1975). *The Mathematics of Diffusion*, 2nd ed. Oxford, UK: Oxford University Press.

Doran M, Hajnal JV, Van Bruggen N, King MD, Young IR, Bydder GM (1990). Normal and abnormal white matter tracts shown by MR imaging using directional diffusion weighted sequences. *J Comput Assist Tomogr* 14:865–873.

Douek P, Turner R, Pekar J, Patronas N, Le Bihan D (1991). MR color mapping of myelin fiber orientation. *J Comput Assist Tomogr* 15(6):923–929.

Einstein A (1926). *Investigations on the Theory of the Brownian Movement*. New York: Dover Publications.

Frank LR (2001). Anisotropy in high angular resolution diffusion-weighted MRI. *Magn Reson Med* 45(6):935–939.

Frank LR (2002). Characterization of anisotropy in high angular resolution diffusion-weighted MRI. *Magn Reson Med* 47(6):1083–1099.

Garrido L, Wedeen VJ, Kwong KK, Spencer UM, Kantor HL (1994). Anisotropy of water diffusion in the myocardium of the rat. *Circ Res* 74(5):789–793.

Hahn EL (1950). Spin-echoes. *Phys Rev* 80(4):580–594.

Henkelman RM, Stanisz GJ, Kim JK, Bronskill MJ (1994). Anisotropy of NMR properties of tissues. *Magn Reson Med* 32(5):592–601.

Inglis BA, Bossart EL, Buckley DL, Wirth ED, 3rd, Mareci TH (2001). Visualization of neural tissue water compartments using biexponential diffusion tensor MRI. *Magn Reson Med* 45(4):580–587.

Jansons KM, Alexander DC (2003). Persistent angular structure: new insights from diffusion magnetic resonance imaging data. *Invers Probl* 19(5):1031–1046.

Jones DK (2004). The effect of gradient sampling schemes on measures derived from diffusion tensor MRI: a Monte Carlo study. *Magn Reson Med* 51(4):807–815.

Jones DK (2008). Tractography gone wild: probabilistic fibre tracking using the wild bootstrap with diffusion tensor MRI. *IEEE Trans Med Imaging* 27(9):1268–1274.

Jones DK, Basser PJ (2004). "Squashing peanuts and smashing pumpkins": how noise distorts diffusion-weighted MR data. *Magn Reson Med* 52(5):979–993.

Jones DK, Pierpaoli C (2004). Towards a marriage of deterministic and probabilistic tractography methods: bootstrap analysis of fiber trajectories in the human brain. Paper read at the 12th annual meeting of ISMRM, Kyoto, Japan.

Jones DK, Simmons A, Williams SC, Horsfield MA (1999). Non-invasive assessment of axonal fiber connectivity in the human brain via diffusion tensor MRI. *Magn Reson Med* 42(1):37–41.

Kärger J, Pfeifer H, Heink W (1988). Principles and applications of self-diffusion measurements by nuclear magnetic resonance. In Waugh J (Ed.), *Advances in Magnetic Resonance*. New York: Academic Press.

Koch MA, Norris DG, Hund-Georgiadis M (2002). An investigation of functional and anatomical connectivity using magnetic resonance imaging. *Neuroimage* 16(1):241–250.

Koch M, Glauche V, Finsterbusch J, Nolte U, Frahm J, Büchel C (2001). Estimation of anatomical connectivity from diffusion tensor data. *Neuroimage* 13:S176.

Le Bihan D (1991). Molecular diffusion nuclear magnetic resonance imaging. *Magn Reson Q* 7(1):1–30.

Le Bihan D, Breton E, Lallemand D, Grenier P, Cabanis E, Laval-Jeantet M (1986). MR imaging of intravoxel incoherent motions: application to diffusion and perfusion in neurologic disorders. *Radiology* 161(2): 401–407.

Le Bihan D, Delannoy J, Levin RL (1989). Temperature mapping with MR imaging of molecular diffusion: application to hyperthermia. *Radiology* 171(3):853–857.

Liu CL, Bammer R, Moseley ME (2003). Generalized diffusion tensor imaging (GDTI): a method for characterizing and imaging diffusion anisotropy caused by non-Gaussian diffusion. *Israel J Chem* 43(1-2):145–154.

Makris N, Worth AJ, Sorensen AG, Papadimitriou GM, Wu O, Reese TG, Wedeen VJ, Davis TL, Stakes JW, Caviness VS, Kaplan E, Rosen BR, Pandya DN, Kennedy DN (1997). Morphometry of in vivo human white matter association pathways with diffusion-weighted magnetic resonance imaging. *Ann Neurol* 42(6):951–962.

Mattiello J, Basser PJ, Le Bihan D (1994). Analytical expression for the b matrix in NMR diffusion imaging and spectroscopy. *J Magn Reson* A 108:131–141.

Mattiello J, Basser PJ, Le Bihan D (1995). Analytical calculation of the b matrix in diffusion imaging. In Le Bihan D (Ed.), *Diffusion and Perfusion Magnetic Resonance Imaging*. New York: Raven Press.

Mattiello J, Basser PJ, Le Bihan D (1997). The b matrix in diffusion tensor echo-planar imaging. *Magn Reson Med* 37(2):292–300.

Mills R (1973). Self-diffusion in normal and heavy water in the range 1–45°. *J Phys Chem* 77(5):685–688.

Moonen CT, Pekar J, de Vleeschouwer MH, van Gelderen P, van Zijl PCM, DesPres D (1991). Restricted and anisotropic displacement of water in healthy cat brain and in stroke studied by NMR diffusion imaging. *Magn Reson Med* 19(2):327–332.

Mori S, Crain BJ, Chacko VP, van Zijl PC (1999). Three-dimensional tracking of axonal projections in the brain by magnetic resonance imaging. *Ann Neurol* 45(2):265–269.

Moseley ME, Cohen Y, Kucharczyk J, Mintorovitch J, Asgari HS, Wendland MF, Tsuruda J, Norman D (1990a). Diffusion-weighted MR imaging of anisotropic water diffusion in cat central nervous system. *Radiology* 176(2):439–445.

Moseley ME, Cohen Y, Mintorovitch J, Chileuitt L, Shimizu H, Kucharczyk J, Wendland MF, Weinstein PR (1990b). Early detection of regional cerebral ischemia in cats: comparison of diffusion- and T2-weighted MRI and spectroscopy. *Magn Reson Med* 14(2):330–346.

Moseley ME, Kucharczyk J, Asgari HS, Norman D (1991). Anisotropy in diffusion-weighted MRI. *Magn Reson Med* 19(2):321–326.

Moseley ME, Kucharczyk J, Mintorovitch J, Cohen Y, Kurhanewicz J, Derugin N, Asgari H, Norman D (1990c). Diffusion-weighted MR imaging of acute stroke: correlation with T2-weighted and magnetic susceptibility-enhanced MR imaging in cats. *AJNR Am J Neuroradiol* 11(3):423–429.

Moseley ME, Mintorovitch J, Cohen Y, Asgari HS, Derugin N, Norman D, Kucharczyk J (1990d). Early detection of ischemic injury: comparison of spectroscopy, diffusion-, T2-, and magnetic susceptibility-weighted MRI in cats. *Acta Neurochir Suppl (Wien)* 51:207–209.

Mulkern RV, Gudbjartsson H, Westin CF, Zengingonul HP, GartnerW, Guttmann CR, Robertson RL, Kyriakos W, Schwartz R, Holtzman D, Jolesz FA, Maier SE (1999). Multi-component apparent diffusion coefficients in human brain. *NMR Biomed* 12(1):51–62.

Neeman M, Freyer JP, Sillerud LO (1990). Pulsed-gradient spin-echo studies in NMR imaging. Effects of the imaging gradients on the determination of diffusion coefficients. *J Magn Reson* 90:303–312.

Neil JJ, Shiran SI, McKinstry RC, Schefft GL, Snyder AZ, Almli CR, Akbudak E, Aronovitz JA, Miller JP, Lee BC, Conturo TE (1998). Normal brain in human newborns: apparent diffusion coefficient and diffusion anisotropy measured by using diffusion tensor MR imaging. *Radiology* 209(1):57–66.

Özarslan E, Mareci TH (2003). Generalized diffusion tensor imaging and analytical relationships between diffusion tensor imaging and high angular resolution diffusion imaging. *Magn Reson Med* 50(5):955–965.

Özarslan E, Shepherd TM, Vemuri BC, Blackband SJ, Mareci TH (2006). Resolution of complex tissue microarchitecture using the diffusion orientation transform (DOT). *Neuroimage* 31(3):1086–1103.

Özarslan E, Vemuri BC, Mareci TH (2005). Generalized scalar measures for diffusion MRI using trace, variance, and entropy. *Magn Reson Med* 53(4):866–876.

Pajevic S, Aldroubi A, Basser PJ (2002). A continuous tensor field approximation of discrete DT-MRI data for extracting microstructural and architectural features of tissue. *J Magn Reson* 154(1):85–100.

Pajevic S, Basser PJ (2003). Parametric and non-parametric statistical analysis of DT-MRI data. *J Magn Reson* 161(1):1–14.

Pajevic S, Pierpaoli C (1999). Color schemes to represent the orientation of anisotropic tissues from diffusion tensor data: application to white matter fiber tract mapping in the human brain. *Magn Reson Med* 42(3): 526–540.

Pajevic S, Pierpaoli C (2000). Color schemes to represent the orientation of anisotropic tissues from diffusion tensor data: application to white matter fiber tract mapping in the human brain. *Magn Reson Med* 43(6):921.

Parker GJ, Wheeler-Kingshott CA, Barker GJ (2002). Estimating distributed anatomical connectivity using fast marching methods and diffusion tensor imaging. *IEEE Trans Med Imaging* 21(5):505–512.

Parker GJM (2000). Tracing fibre tracts using fast marching. Paper read at the 8th annual meeting of the ISMRM, Denver, CO.

Peled S, Cory DG, Raymond SA, Kirschner DA, Jolesz FA (1999). Water diffusion, T(2), and compartmentation in frog sciatic nerve. *Magn Reson Med* 42(5):911–918.

Pierpaoli C, Barnett A, Pajevic S, Chen R, Penix LR, Virta A, Basser PJ (2001). Water diffusion changes in Wallerian degeneration and their dependence on white matter architecture. *Neuroimage* 13 (6 Pt 1):1174–1185.

Pierpaoli C, Basser PJ (1996). Toward a quantitative assessment of diffusion anisotropy [published erratum appears in *Magn Reson Med* 1997 Jun;37(6):972]. *Magn Reson Med* 36(6):893–906.

Pierpaoli C, Jezzard P, Basser PJ, Barnett A, Di Chiro G (1996). Diffusion tensor MR imaging of the human brain. *Radiology* 201(3):637–648.

Poupon C, Clark CA, Frouin V, Bloch I, Le Bihan D, Mangin J-F (1999). Tracking white matter fascicles with diffusion tensor imaging. Paper read at the 7th annual meeting of the ISMRM, Philadelphia.

Poupon F, Mangin JF, Hasboun D, et al. (1998). Multi-object deformable templates dedicated to the segmentation of brain deep structures. *Lect Notes Comput S C* 1496:1134–1143.

Reese TG, Heid O, Weisskoff RM, Wedeen VJ (2003). Reduction of eddy-current-induced distortion in diffusion MRI using a twice-refocused spin echo. *Magn Reson Med* 49(1):177–182.

Rohde GK, Barnett AS, Basser PJ, Marenco S, Pierpaoli C (2004). Comprehensive approach for correction of motion and distortion in diffusion-weighted MRI. *Magn Reson Med* 51(1):103–114.

Sakuma H, Nomura Y, Takeda K, Tagami T, Nakagawa T, Tamagawa Y, Ishii Y, Tsukamoto T (1991). Adult and neonatal human brain: diffusional anisotropy and myelination with diffusion-weighted MR imaging. *Radiology* 180(1):229–233.

Simpson JH, Carr HY (1958). Diffusion and nuclear spin relaxation in water. *Phys Rev* 111(5):1201–1202.

Stejskal EO (1965). Use of spin echoes in a pulsed magnetic-field gradient to study anisotropic restricted diffusion and flow. *J Chem Phys* 43(10):3597–3603.

Stejskal EO, Tanner JE (1965). Spin diffusion measurements: spin echoes in the presence of time-dependent field gradient. *J Chem Phys* 42(1): 288–292.

Stepisnik J (1999). Validity limits of Gaussian approximation in cumulant expansion for diffusion attenuation of spin echo. *Physica B* 270: 110–117.

Tanner JE (1966). Use of a pulsed magnetic-field gradient for measurements of self-diffusion by spin-echo nuclear magnetic resonance with applications to restricted diffusion in several tissues and emulsions. Ph.D. thesis in chemistry, physics, University of Wisconsin, Madison, WI.

Tanner JE (1977). Self-diffusion in cells and tissues. In *Annual Report*. Crane, Ind Naval Weapons Support Center.

Tanner JE (1978). Transient diffusion in system partitioned by permeable barriers. Application to NMR measurements with a pulsed field gradient. *J Chem Phys* 69(4):1748–1754.

Tanner JE (1979). Self-diffusion of water in frog muscle. *Biophys J* 28(1): 107–116.

Tanner JE (1983). Intracellular diffusion of water. *Arch Biochem Biophys* 224(2):416–428.

Torrey HC (1956). Bloch equations with diffusion terms. *Phys Rev* 104(3):563–565.

Tuch DS, Belliveau JW, Wedeen V (2000). A path integral approach to white matter tractography. Paper read at the 8th annual meeting of the ISMRM, Denver, Colorado.

Tuch DS, Reese TG, Wiegell MR, Wedeen VJ (2003). Diffusion MRI of complex neural architecture. *Neuron* 40(5):885–895.

Turner R, Le Bihan D, Maier J, Vavrek R, Hedges LK, Pekar J (1990). Echo-planar imaging of intravoxel incoherent motion. *Radiology* 177 (2): 407–414.

Ulug AM, Beauchamp N, Bryan RN, van Zijl PCM (1997). Absolute quantitation of diffusion constants in human stroke. *Stroke* 28:483–490.

van Gelderen P, de Vleeschouwer MHM, DesPres D, Pekar J, van Zijl PCM, Moonen CTW (1994). Water diffusion and acute stroke. *Magn Reson Med* 31:154–163.

Warach S, Chien D, Li W, Ronthal M, Edelman RR (1992). Fast magnetic resonance diffusion-weighted imaging of acute human stroke [published erratum appears in Neurology 1992 Nov;42(11):2192]. *Neurology* 42(9):1717–1723.

Warach S, Gaa J, Siewert B, Wielopolski P, Edelman RR (1995). Acute human stroke studied by whole brain echo planar diffusion-weighted magnetic resonance imaging. *Ann Neurol* 37(2):231–241.

Wedeen VJ, Reese TG, Tuch DS, Weigel MR, Dou J-G, Weiskoff RM, Chessler D (2000). Mapping fiber orientation spectra in cerebral white matter with Fourier-transform diffusion MRI. Paper read at the 8th Annual Meeting of the ISMRM, Denver, Colorado.

Wedeen VJ, Davis TL, Weisskoff RM, Tootell R, Rosen BR, Belliveau JW (1995). White matter connectivity explored by MRI. Paper read at the Proceedings of the First International Conference for Functional Mapping of the Human Brain, Paris.

Westin C-F, Maier S, Khidir B, Everett P, Jolesz FA, Kikinis R (1999). Image processing for diffusion tensor magnetic resonance imaging. Paper read at MICCAI '99, Cambridge, UK.

Wimberger DM, Roberts TP, Barkovich AJ, Prayer LM, Moseley ME, Kucharczyk J (1995). Identification of premyelination by diffusion-weighted MRI. *J Comput Assist Tomogr* 19(1):28–33.

Zhang S, Bastin ME, Laidlaw DH, Sinha S, Armitage PA, Deisboeck TS (2004). Visualization and analysis of white matter structural asymmetry in diffusion tensor MRI data. *Magn Reson Med* 51(1):140–147.

Zhang S, Curry C, Morris DS, Laidlaw DH (2000). Visualizing diffusion tensor MR images using streamtubes and streamsurfaces. Paper read at Proceedings of the IEEE Visualization Conference, Utah.